CRYSTAL GROWTH & DESIGN

pubs.acs.org/crystal

Article

Mononuclear Lanthanide Complexes in Triangular Dodecahedron Geometry: Manifestation of Single Ion Magnet Behavior for Dy^{III} Analogue

Published as part of a Crystal Growth and Design virtual special issue on Molecular Magnets and Switchable Magnetic Materials

Soumalya Roy, Jiyuan Du, Ezhava Manu Manohar, Lin Sun,* Naushad Ahmed,* Atanu Dey,* and Sourav Das*

Cite This: *Cryst. Growth Des.* 2023, 23, 1066−1075

Read Online

ABSTRACT: In this work, a tridentate *N,N,O* ligand [(*E*)-4-nitro-2-((pyridine-2-ylmethylene)amino)phenol] ($L_{NO2}H$) is employed for the synthesis of neutral structurally similar complexes $[Dy^{III}(L_{NO2})_2(Cl)(H_2O)]\bullet H_2O$ (**1**) and $[Er^{III}(L_{NO2})_2(Cl)(CH_3OH)]\bullet 3CH_3OH$ (**2**). Both complexes are characterized by single-crystal X-ray diffraction studies. Ln^{III} ion in complexes **1** and **2** is eight coordinated and possesses triangular dodecahedron geometry as confirmed by the SHAPE analysis. The Hirshfeld surface calculation emphasizes the importance of hydrogen bond interaction that controls the overall crystal packing. The magnetic studies reveal that complex **1** shows single ion magnet (SIM) behavior with an effective energy barrier of 34.16 K and pre-exponential parameter 6.51×10^{-6} s. The CASSCF based *ab initio* calculations were performed on complexes **1** and **2** to extract SH parameters and the plausible magnetic relaxation dynamics.

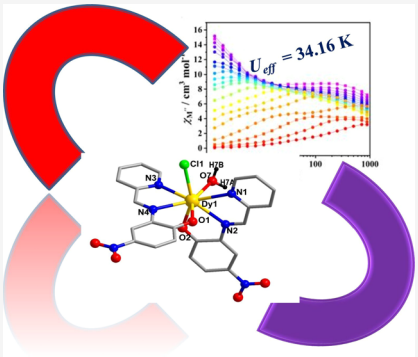

INTRODUCTION

Much attention has recently been drawn to the lanthanide complexes because of their versatile applications in the field of catalysis,[1,2] photophysical properties,[3−6] and magnetic materials.[7−11] Magnetic materials consisting of transition metal (3d) and/or lanthanide (4f) ions have promising applications in terms of data storage, low temperature magnetic refrigerant, spintronics, etc.[12−18] Initially, the field was restricted in the synthesis of multinuclear complexes containing 3d, 3d/4f, and 4f metal ions for achieving the larger ground (S) in the aim for a high energy barrier [$U_{eff} = |D|S^2$] for spin reversal.[19−27] Later on, realizing the fact that anisotropy (D) is inversely proportional to the square of total spin (S) of the complex, the research direction was shifted toward the synthesis of a mononuclear single molecule magnet or single ion magnet (MSMM or SIM).[28−35] Another important phenomenon that boosted the field toward the MSMM is to rationalize the structure property relationship through theoretical calculations.[36−39] The correlation of the magnetic properties with the geometry in MSMM becomes simpler compared to the polynuclear complexes.[39−50] MSMMs particularly containing lanthanide ions have attained a special interest due to the strong spin−orbit coupling (SOC) for lanthanides that invoke a large magnetic anisotropy in lanthanide-based complexes.[51−54] The field was embarked by Ishikawa and co-workers through the complex $(Bu_4N)[Ln(Pc)_2]$ (Ln^{III} = Tb and Dy; Pc = phthalocyaninato) in 2003.[55] Recent examples by Layfield and others have accelerated the quest for lanthanide based complexes as molecular magnets.[56,57] However, the ground state intrinsic quantum tunneling of magnetization (QTM) that shortcuts the path for relaxation of magnetization acts as a barrier in lanthanide-based complexes.[58−61] Theoretical calculations by Chibotaru and co-workers demonstrate the effect of the symmetry of the lanthanide complexes on the QTM.[59,62] The higher symmetry in lanthanide complexes restricts the mixing of $\pm M_J$ states and thereby reduces the ground state QTM.[63−70] Among these lanthanide-based complexes, the Kramer's ions Dy^{III} and Er^{III} are of appealing interest due to their intrinsic magnetic-bistable ground states.[71−74] Moreover, based on the electrostatic model for the enhancement of the single ion anisotropy as proposed by Long and co-workers, Dy^{III} and Er^{III} ions are of contrasting characteristics.[75] Dy^{III} ion being oblate in nature prefers ligand

Received: October 28, 2022
Revised: December 22, 2022
Published: January 16, 2023

https://doi.org/10.1021/acs.cgd.2c01226
Cryst. Growth Des. 2023, 23, 1066−1075

coordination from the axial position, where the prolate ion Er^{III} prefers ligation from the equatorial plane.[76−79] Consequently, this will provide a platform to check the ligation possibility of a particular ligand for these two lanthanide ions. In this line of interest we intend to check the fecundity of a tridentate ligand, [(*E*)-4-nitro-2-((pyridine-2-ylmethylene)amino)phenol] ($L^{NO2}H$) toward Dy^{III} and Er^{III} ions. Accordingly the reaction of $L_{NO2}H$ with $LnCl_3$ (Ln^{III} = Dy^{III},Er^{III}) precursors leads to the formation of complexes $[Dy^{III}(L_{NO2})_2(Cl)(H_2O)]\bullet H_2O$ (**1**) and $[Er^{III}(L_{NO2})_2(Cl)(CH_3OH)]\bullet 3CH_3OH$ (**2**). Magnetic studies reveal that complex **1** exhibits SIM behavior, while complex **2** does not show slow magnetic relaxation behavior. Meanwhile, the differences of the magnetic behaviors for the two complexes have been explained by the CASSCF based *ab initio* calculations.

■ EXPERIMENTAL SECTION

Reagents and General Procedures. *All the Reagents and Chemicals Were Purchased from Commercial Source Were Used without Further Purification.* 2-Pyridinecarboxyaldehyde (99%, 1121−60−4), 2-amino-4-nitrophenol (96%, 99−57−0), $DyCl_3\cdot 6H_2O$ (99.99%,15059−52−6), $ErCl_3\cdot 6H_2O$ (99.99%, 10025−75−9), Sigma-Aldrich Chemical Co. (U.S.A.). Solvents were reagent grade and distilled under nitrogen prior to their use. All other chemicals were reagent grade, available commercially, and used as received.

Instrumentation. IR data were collected in the range of 450−4500 cm^{-1} using a PerkinElmer Spectrum two FTIR Spectrometer with an ATR module. Elemental analysis was done using Carlo Erba EA 1108 analyzer.

Magnetic Measurements. Magnetic measurements were performed in the temperature range 2−300 K with an applied field of 1000 Oe, using a Quantum Design MPMS-XL-7 SQUID magnetometer on polycrystalline samples. The diamagnetic corrections for compounds were estimated using Pascal's constants. Alternating current (ac) susceptibility experiments were performed using an oscillating ac field of 2.0 Oe at ac frequencies ranging from 1 to 1000 Hz. The magnetization was measured in the field range 0−7 T.

X-ray Crystallography. Single crystal X-ray data of compounds **1**-**2** were collected from Bruker Kappa APEXII diffractometer having graphite-monochromatic with MoKα radiation (λ = 0.71073 Å). The structures were solved by software packages SMART,[80] SAINT,[81] SADABS,[81] and SHELXTL[82,83]and refined by the full matrix least-squares of F^2 using the SHELXL-2014[83] along with Olex-2 software.[84] Anisotropic thermal parameters were assigned to all non-hydrogen atoms. Diamond 3.1e software[85] was used to design the crystal structure. The crystallographic data and parameters are presented in Table S1. X-ray data can be accessed through the CCDC [complex **1**2205551; complex **2**2205552] and can be obtained from www.ccdc.cam.ac.uk/data_request/cif.

Synthesis of $L_{NO2}H$. The synthesis method of ligand $L_{NO2}H$ was obtained from previous literature.[86]

General Synthesis Procedure of Complexes 1 and 2. The Ligand $L_{NO2}H$ is dissolved in $MeOH/CHCl_3$ (30 mL, 1:1) solvent and stirred for 1 h. $LnCl_3\bullet xH_2O$ (Ln^{III} = Dy^{III}, Er^{III}) and triethylamine are added to the reaction mixture and again stirred for 12 h at room temperature. The reaction mixture is filtered out, and the precipitate is dissolved in $MeOH/CHCl_3$ (1:1). Red, block-shaped crystals suitable for single crystal X-ray diffraction are obtained by slow evaporation. The particulars for both the complexes and characterization data are enlisted below.

$[Dy(L_{NO2})_2(Cl)(H_2O)]\bullet H_2O$ (1). Quantities: $L_{NO2}H$ (0.040 g, 0.18 mmol), $DyCl_3\bullet 6H_2O$ (0.071 g, 0.18 mmol), Et_3N (0.079 mL, 0.78 mmol), Yield: 0.036 g, 35% (based on Dy^{3+}). Anal. Calcd for $C_{24}H_{20}ClDyN_6O_8$ (718.41): Calcd: C, 40.13; H, 2.81; N, 11.70; Found: C, 40.32; H, 2.92; N, 11.84; IR (KBr) (cm^{-1}): 1616.86(s), 1564.27(s), 1483.84(s), 1360.80(s), 1297.20(m), 1173.46(m), 1021.88(m), 906.39(m).

$[Er^{III}(L_{NO2})_2(Cl)(CH_3OH)]\bullet 3CH_3OH$ (2). Quantities: $L_{NO2}H$ (0.040 g, 0.18 mmol), $ErCl_3\bullet 6H_2O$ (0.071 g, 0.18 mmol), Et_3N (0.079 mL, 0.78 mmol), Yield: 0.036 g, 35% (based on Er^{3+}). Anal. Calcd For$C_{28}H_{32}ClErN_6O_{10}$ (815.30): Cald: C, 41.25; H, 3.96, N, 10.31; Found: C, 41.31; H, 4.03; N, 10.44; IR (KBr) (cm^{-1}):1643.67(s), 1599.33(s), 1475.59(s), 1985.88(s), 1279.67(m), 1164.18(m), 1075.50(m), 969.29(m).

■ RESULTS AND DISCUSSION

Synthesis Aspect. The efficacy of the salicyldehyde containing hydrazone-based ligands in constructing molecular lanthanide complexes is well-explored. Utilizing this concept, we have designed the *N,N,O* ligand ((*E*)-4-nitro-2-((pyridine-2-ylmethylene)amino)phenol) ($L_{NO2}H$).[87] We envisaged that three flexible *N,N,O* coordinating sites of the ligand can bind with the lanthanide ion. The coordination of two such monoanionic ligands (L_{NO2}^-) along with the halide ion can generate hepta-coordination around the Ln^{III} center. It is well-documented that complexes with high symmetry such as D_{6h}, D_{5h}, D_{4h}, D_{4d}, D_∞, and S_8 are promising candidates for constructing molecular magnets with high performance as the higher symmetries prevent the mixing of wave functions and thereby quench the QTM.[88−93] Accordingly $L_{NO2}H$ reacts with $LnCl_3\bullet 6H_2O$ (Ln = Dy^{III}, Er^{III}) in the presence of triethylamine to yield mononuclear complexes $[Dy^{III}(L_{NO2})_2(Cl)(H_2O)]\bullet H_2O$ (**1**) and $[Er^{III}(L_{NO2})_2(Cl)(CH_3OH)]\bullet 2CH_3OH$ (**2**). However, in these complexes Ln^{III} centers are eight coordinated due to an additional coordination from water in complex **1** and MeOH in complex **2** (Scheme-1).

Scheme 1. General Synthetic Route to Isolate 1 and 2

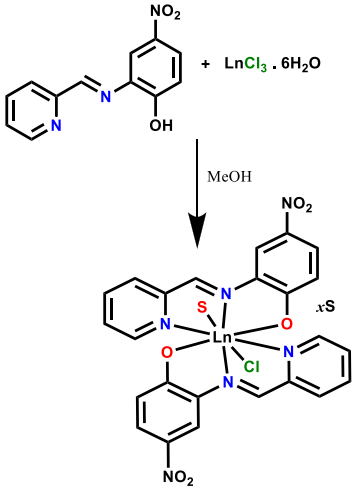

Single Crystal X-ray Analysis of $[Dy(L_{NO2})_2(Cl)(H_2O)]\bullet H_2O$ (1). Single crystal XRD studies show that complexes **1** and **2** are neutral and crystallize in triclinic system with $P\bar{1}$ (Z = 2) space group. The molecular structure of complex **1** is analogous to that of complex **2** with minor differences. In complex **1**, aqua ligand is coordinated with the Dy^{III} center, whereas in complex **2** methanol is coordinated with the Er^{III} center. The molecular structures for complexes **1** and **2** are provided in Figures 1 and S1. The detailed structural parameters are listed in Tables S2 and S3 for **1** and **2**, respectively. Due to the analogous molecular entity, we have described the structural details for complex **1**.

https://doi.org/10.1021/acs.cgd.2c01226
Cryst. Growth Des. 2023, 23, 1066−1075

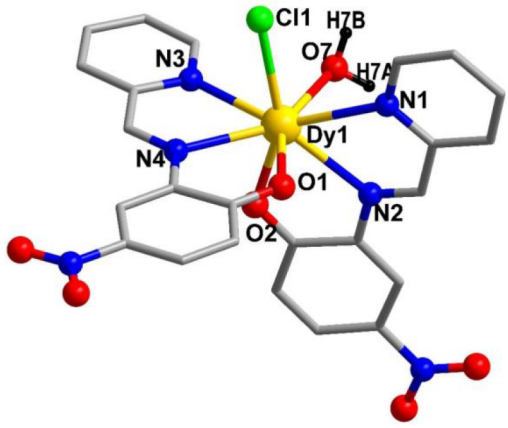

Figure 1. Crystal structure of complex **1** (H atoms ware omitted for the clarity apart from coordinated H_2O molecule).

The asymmetric unit of complex **1** consists of one Dy^{III} ion, two deprotonated $[L_{NO2}]^-$ ligand, one Cl^- ion, and one aqua ligand. Each ligand adopts μ_1-η^1:η^1:η^1 coordination mode in its deprotonated form. The phenolate ion of the ligand binds more strongly with the Dy^{III} ion due to the oxophilic nature of the lanthanide ion [Dy^{III}−$O_{phenolate}$= 2.325(3) and 2.273(2) Å]. The imino-nitrogen of the ligand coordinates to the Dy^{III} center with a distance of Dy^{III}−N_{imine} = 2.495(3) and 2.537(3) Å. The imino-nitrogen binds more strongly to the Dy^{III} ion compared to the pyridine nitrogen Dy^{III}−$N_{pyridine}$ = 2.65(3) and 2.614(3) Å. The terminally coordinated chloride and aqua ligand with the central metal ion generate eight-coordinated Dy^{III} center (Figure S2). The bond distances related to chloride and aqua ligand are Dy^{III}−Cl = 2.641(1) Å and Dy^{III}−O_{water} = 2.399(3) Å. SHAPE analysis confirms the triangular dodecahedron (D_{2d}) geometry around the central metal ion in both **1** and **2** (Table S4).[94] A close inspection of the packing diagram for these complexes reveals the shortest Ln---Ln separations of 7.734 Å (Figure S4). The metric parameters involved in **1** and **2** are provided in Table 1 which are relevant to literature precedents.

Table 1. Comparison of Bond Distances in Complexes 1 and 2

	1	2
Ln−$N_{pyridine}$	2.65(3); 2.614(3)	2.588(3); 2.612(3)
Ln−N_{imine}	2.495(3); 2.537(3)	2.464(4); 2.486(4)
Ln−$O_{phenolate}$	2.325(3); 2.273(2)	2.309(3); 2.27(2)
Ln−Cl	2.641(1)	2.636(1)
Ln−$O_{solvent}$	2.399(3)	2.334(2)
Shortest Ln^{III}---Ln^{III} separation	7.734(5)	7.734(2)

The bulk phase purity for these complexes is confirmed through PXRD analysis (Figure S5). The differences in peak intensity may be due to the preferred orientation of the powdered samples.

Hirshfeld Surface Analysis on 1 and 2. There are several reports indicating the inter- and intramolecular interactions can influence the dynamic magnetic behavior of metal complexes[95] In this line of interest we intended to understand the interactions present in complexes **1** and **2**. We have performed Hirshfeld surface analysis on complexes **1** and **2** using CrystalExplorer 21.5 software.[96] The Hirshfeld surface was mapped in $d_{norm}$for complexes **1** (Figure 2) and **2** (Figure S6). The d_e and d_i have their usual meaning about nearest distance from outside and inside molecules from the Hirshfeld surface, respectively. In the case of **1** major intermolecular interactions (∼32.6%) are found through hydrogen bonds H···O/O···H in the range of 1.48 Å intermolecular distance (coordinated water and water molecule present in the crystal lattice) and the second major interaction (25.3%) is found through H···H. In the case of **2** the major interactions are found through H···H (32.2% Figure S5) and the second major interaction through H···O/O···H (29.5%) in the range of intermolecular distance of 1.76 Å. This difference in the major interactions observed in the cases of **1** and **2** is mainly due to the type of coordinated and crystal lattice solvent molecules (in case of **1** water molecule while in the case of **2** methanol). In both the cases the C···H interactions (inside and outside of the surface molecules) were found to be ∼6%. We have also reported other weak interactions by mapping in shape index, curvedness, fragment patch, etc. (Figure 3 and Figure S7). The asphericity value which is indicative of structural anisotropy was found to be 0.021 and 0.033, respectively, in the cases of **1**and **2**.

Magnetic Properties of 1 and 2. Direct current (dc) magnetic susceptibility measurements for complexes **1** and **2** have been carried out from 300 to 2 K under an applied magnetic field of 1 k*Oe* (Figure 4). The room temperature $\chi_M T$ values of 14.14 cm^3 K mol^{-1} (for **1**) and 11.90 cm^3 K mol^{-1} (for **2**) are close to the expected values for a Dy^{III} ion and Er^{III} ion (14.17 cm^3 K mol^{-1}, $^6H_{15/2}$, S = 5/2, L = 5, g = 4/3 for Dy^{III} ion, 11.48 cm^3 K mol^{-1}, $^4I_{15/2}$, S = 3/2, L = 6, g = 6/5 for Er^{III} ion). It worth noting that the $\chi_M T$ values of two complexes fall steadily with cooling before dropping rapidly to just 9.33 cm^3 K mol^{-1} for complex **1** and 4.43 cm^3 K mol^{-1} for complex **2** at 2 K, respectively. The decrease in $\chi_M T$ value can be attributed to the progressive depopulation of the Dy^{III}/Er^{III} ion excited Stark sublevels and/or the possible intermolecular antiferromagnetic interactions between neighboring Dy^{III}/Er^{III} ions at low temperature.[97,98]

The field dependent magnetization data at 2 , 3, and 5 K for complexes **1** and **2** were collected in field sweep ranges of 0−70 k*Oe* (Figure S8). The magnetization data of **1** and **2** go up moderately with increasing applied dc field, reaching the maximum magnetization values of 6.89 $N\beta$ (**1**) and 8.37 Nβ (**2**) at 70 k*Oe*, respectively, which deviate from the theoretical saturation value (10 $N\beta$ for complex **1** and 9 $N\beta$ for complex **2**), possibly owing to the presence of large magnetic anisotropy, crystal-field effect, and/or low-lying excited states.[99,100]

Meanwhile, the nonoverlapping nature of reduced magnetization (M versus H/T) curves (Figure S8) further implies the presence of low-lying excited states and/or significant magnetic anisotropy.[101,102]

To further explore the magnetic dynamic behavior of **1** and **2**, the alternating-current (ac) susceptibility measurements were carried out. Frequency-dependent ac susceptibility measurements show that **1** exhibits SIM behavior under zero dc field, while the maximum values of out-of-phase (χ_M'') signals increase as temperature declines, suggesting the presence of strong QTM between the ground Kramers doublets at low temperature[103,104] (Figure S9). However, no peaks of the ac susceptibility χ_M'' of **2** can be observed at zero dc field (Figure S10). Therefore, ac susceptibility measurements for **1** were tested at increasing fields from 0 to 4 k*Oe* at 2.0 K suppressing QTM by imposing the optimal dc field

https://doi.org/10.1021/acs.cgd.2c01226
Cryst. Growth Des. 2023, 23, 1066−1075

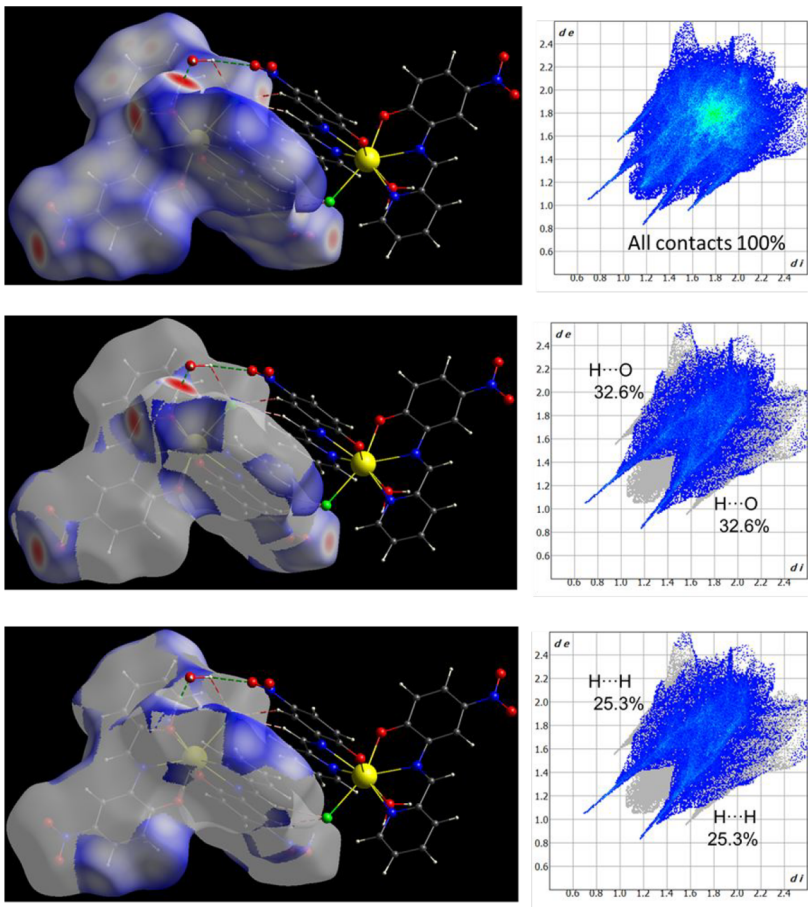

Figure 2. Hirshfeld surface mapped in 3D d_{norm}. Surface plots (left) and the major intermolecular interactions (right) shown by 2D fingerprint for complex **1**. The interactions through H-bonding are shown in green dotted lines and through short contacts as brown dotted lines. Note: Short contacts and long contacts are represented by the red and blue areas, respectively. White area represents contacts with lengths equivalent to the sum of the van der Waal radii of the interacting atoms.

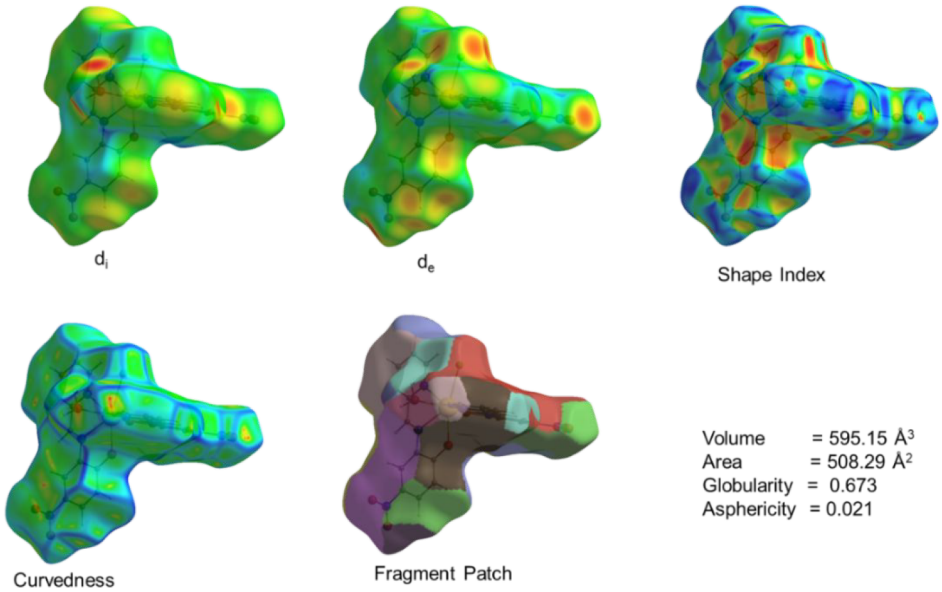

Figure 3. Different view of Hirshfeld surface for **1** indicating the presence of weak intermolecular interactions.

(Figure S11). The maximum relaxation time (τ) was obtained under 1.5 k*Oe*, implying that the QTM could be suppressed effectively. Several out-of-phase (χ_M'') peaks are distinctly observable, and they shift gradually from low frequency to high frequency as temperature increases (Figure 5). Meanwhile, the τ values were derived from the fit of out-of-phase χ_M'' peaks, and the effective energy barrier (U_{eff}) of **1** was obtained by fitting data at the high temperature region with the Arrhenius

https://doi.org/10.1021/acs.cgd.2c01226
Cryst. Growth Des. 2023, 23, 1066−1075

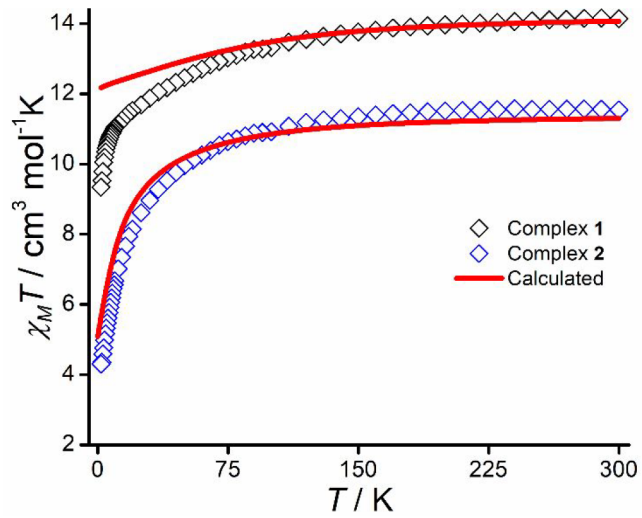

Figure 4. $\chi_M T$ versus T plots for **1** and **2** at 1 k*Oe*.

law: $\tau^{-1} = \tau_0^{-1} \exp(-U_{eff}/kT)$, giving parameters U_{eff}/k = 34.16 K and $\tau_0 = 6.51 \times 10^{-6}$ s (Figure 5c). Notably, the Cole−Cole plots for **1** on the basis of frequency-dependent ac susceptibility data are far from a semicircular shape below the 5.0 K owing to the presence of competing relaxation processes like Raman process, direct process, and thermally assisted quantum tunneling of magnetization (TA-QTM) process.[105] To have a quantitative evaluation of their SMM behavior, the normalized Argand plot of **1** was further obtained from the frequency-dependent ac susceptibility data by fitting with Debye model (Figure S12 and Table S5).[106] The calculated parameters (α) in the range of 0.39−0.72 are relatively large, suggesting the relatively wide distribution of the relaxation process in **1**. Meanwhile, the ratio between the isothermal and adiabatic susceptibilities (χ_T and χ_S) based on the equaction $\chi_T - \chi_S/\chi_T$ indicates that a relatively large fraction of **1** exhibits the slow relaxation of the magnetization behavior (around 90%).[107−109] In the case of **2**, despite the fact that under a dc field of 2000 Oe out-of-phase signals are detected, no maxima are observed, failing to fit the energy barrier (Figure S13).

Computational Studies on Complexes 1 and 2. To rationalize the observed magnetic behavior and to extract SH parameters associated with complexes **1** and **2**, we have performed *ab initio* calculations on the X-ray structures using the MOLCAS 8.2 program.[110] The ANO-RCC basis set for each atom used in our calculation is given in Table S7. To obtained energy of the spin free and spin−orbit states for Dy^{III} (complex **1**) and Er^{III} (complex **2**) having 9 and 11 electrons spanning their seven 4f orbitals, we have computed CAS (9,7) and CAS (11,7), respectively. The computed spin-free and low-lying spin−orbit states for complexes **1** and **2** are provided in Table S8. The energy of eight low-lying spin−orbit state spans up to 441 cm^{-1} for complex **1** and 225 cm^{-1} for complex **2**. Finally, to obtain g-tenors, energy of the low-lying KDs, and magnetic relaxation mechanism, we have performed SINGLE_ANISO calculations. The obtained g-tensors (g_x = 0.0280, g_y = 0.0441, g_z = 19.7341) for ground state KD1 in the case of **1** suggest that the Dy^{III} ion exhibits a slightly axial nature ($g_z \approx 20$) along with transverse component g_x; $g_y \neq 0$. Due to the presence of active transverse components, the

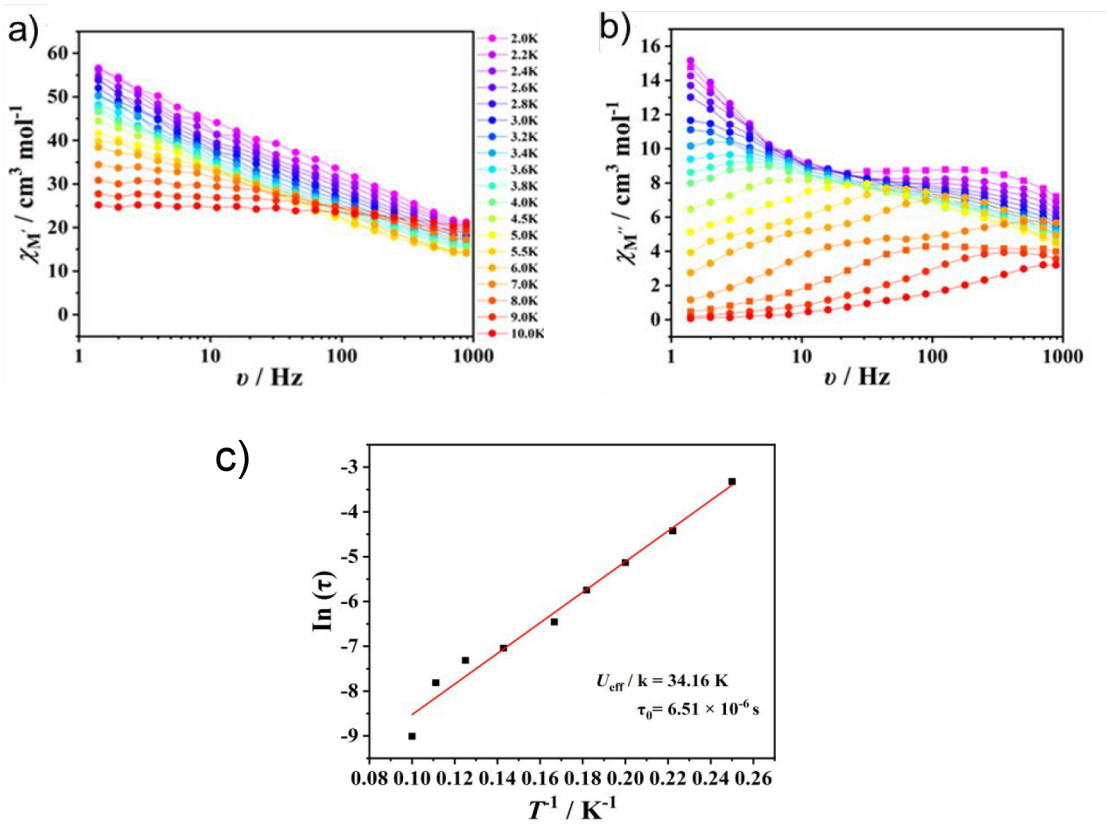

Figure 5. Frequency dependent in-phase (a) and out-of-phase (b) ac magnetic susceptibility data under 1.5 k*Oe* magnetic field for complex **1**. Fit of Cole−Cole plot (c) Arrhenius plot ($\ln(\tau) = f(T^{-1})$) to extract effective energy barrier for spin reversal.

https://doi.org/10.1021/acs.cgd.2c01226
Cryst. Growth Des. 2023, 23, 1066−1075

energy of the eight computed KDs (originated from $^6H_{15}$) was found to span from zero to only 441 cm^{-1} (Table 2). The first excited state (KD2) was separated by 156 cm^{-1} from the ground state (KD1). To shed light on the purity of magnetic ground state ± mJ = 15/2 and strength of admixing with excited ± mJ states of Dy^{III} ion in complex **1**, we have computed and analyze wave function decomposition. The ground magnetic state ± mJ = 15/2 of Dy^{III} in **1** found to be 95% (Table S10, Figure 6) pure and slightly mixed with excited state ± mJ = 11/2 by 3%. The admixing of ground state ± mJ with excited states reflects that the crystal field effect on Dy^{III} is slightly weak, which in turn leads the transverse magnetic anisotropy. Further, we have computed crystal field parameters using $\widehat{H_{CF}} = \sum\sum_{k=-q}^{q} B_k^q O_k^q$ Hamiltonian (where B_k^q and O_k^qparameters are the crystal field parameters and Stevens' operator, respectively).

Table 2. SINGLE_ANISO Computed Energy (cm^{-1}) of the Low-Lying Kramers Doublets (KDs), and g-Tensors and the Angle between the Ground State and First Excited State g_{zz} Axes

Complex **1**		
±mJ states (from 21 Sextets)	g_{xx}; g_{yy}; g_{zz}	θ (°angle)
0.0000	0.0280; 0.0441; 19.7341	115.11
156.2950	1.2542; 4.5982; 13.8811	
190.9796	1.7837; 4.1019; 10.2274	
270.0368	3.0334; 4.1145; 12.8387	
300.6779	1.1133; 2.4799; 13.4690	
325.8868	2.2193; 3.6387; 11.6675	
382.6825	1.4275; 2.6557; 13.4751	
441.7602	0.3849; 0.8099; 17.7412	
Complex **2**		
±mJ states (from 35 Quartets + 112 Doublets)	g_{xx}; g_{yy}; g_{zz}	θ (°angle)
0.0000	1.8531; 3.8660; 12.0099	97.94
18.3717	2.7648; 3.1302; 9.8429	
54.4284	2.8804; 3.8903; 8.2062	
80.7893	6.8484; 6.0359; 1.7695	
131.6915	0.1351; 2.9722; 11.0482	
200.2606	1.6079; 3.3286; 7.5136	
226.6485	2.7736; 4.8482; 10.1168	
255.7706	0.4578; 3.5704; 14.3459	

From Table S9, the computed crystal field parameters B_2^0 = −1.3, B_2^{-2} = −1.1, B_2^{-1} = 0.99, and B_2^1 = 0.99 further indicate the slight deviation from the axial behavior of Dy^{III} ion in **1**. In the case of **2**, the computed *g*-tensors (g_x = 1.8531, g_y = 3.8660, g_z = 12.0099) indicate the strong deviation from the axial behavior of Er^{III} ion. The computed energy of the low-lying KDs span up to 255 cm^{-1}, and the first excited state KD2 is found to be located at only 18 cm^{-1} from the ground state KD1. The wave function analysis suggests the ground state KD1 (± mJ = 15/2) is 44% and strongly admixed with other excited states (Table S10, Figure 6, right). The crystal field parameters value for **2** (Table S8) further support the nonaxial behavior of Er^{III} ion. As usual the orientation of the main magnetization axis g_{zz} is found to be directed toward the Cl^- ligand which consist highest charge density −0.87 following Cl1−Dy1−O1 axis (O1, charge density −0.83, ∠Cl−Dy−O1 = 152.87°) (Figure 6). The orientation of the main magnetization axis slightly deviated from the Dy−Cl1 bond by an angle of ∠Cl−Dy−O1 = 11° while the g_{zz} orientation on Er^{III} ion in **2** strongly deviated by an angle of 53° due to its prolate nature. The plausible mechanism for the reversal of magnetization was shown in Figure 6. The computed moderate transition magnetic moment μ_B = 0.12 × 10^{-01} between the ground state doublet KD1 suggests SIM behavior of **1** with small amount of QTM. A small dc field of H_{dc} = 1.5 k*Oe* was required to suppress the QTM, thus getting the well resolved out-of-phase signals with slowest magnetic relaxation. The observed energy barrier of 34.16 K was found to be low as compared to the *ab initio* blockade barrier of 224.5 K (156 cm^{-1}). In the case of **2**, the computed transition magnetic moment μ_B = 0.95 × 10^{00} suggests magnetic relaxation will occur within the ground state KD1 through fast magnetic tunneling and hence no SIM behavior predicted. Our theoretical studies on complexes **1** and **2** further confirm the SIM behavior of complex **1** and no SIM behavior for complex **2**.

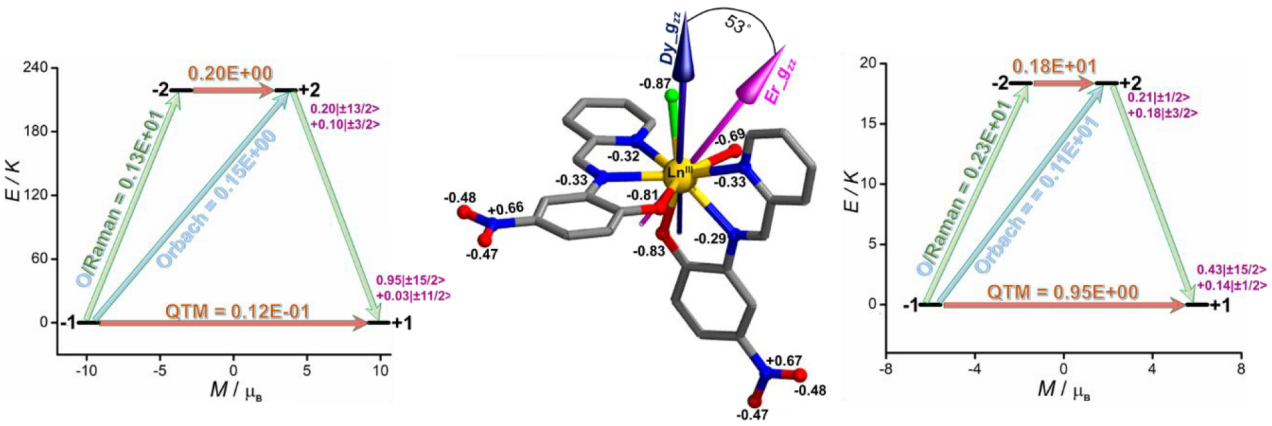

Figure 6. SINGLE_ANISO computed main magnetization axes on lanthanide ions (Dy^{III} and Er^{III}) in their respective complexes **1** and **2**. The plausible magnetic relaxation mechanism (left for **1** and right for **2**). The computed LoProp charges are shown for the coordinated donor atoms of the ligands.

https://doi.org/10.1021/acs.cgd.2c01226
Cryst. Growth Des. 2023, 23, 1066−1075

CONCLUSION

In summary, we have utilized a tridentate *N,N,O* ligand [(*E*)-4-nitro-2-((pyridine-2-ylmethylene)amino)phenol] to isolate metal complexes **1** and **2** with Dy^{III} and Er^{III}, respectively. Two Schiff-base ligands along with a Cl^- and a water or methanol molecule surround Ln^{III} ions and create triangular dodecahedron geometry around Ln^{III} metal ions. The detailed dc and ac magnetic susceptibility measurements reveal that **1** with oblate Dy^{III} ion behaves as a SIM while complex **2** with prolate Er^{III} lacks SIM property. Further *ab initio* theoretical studies on the X-ray structures of complexes **1** and **2** justify the suitable electronic structure around oblate Dy^{III} ion which seems very important to exhibit the slow magnetic relaxation behavior.

ASSOCIATED CONTENT

Supporting Information

The Supporting Information is available free of charge at https://pubs.acs.org/doi/10.1021/acs.cgd.2c01226.

ESI, X-ray data (PDF)

Accession Codes

CCDC 2205551−2205552 contain the supplementary crystallographic data for this paper. These data can be obtained free of charge via www.ccdc.cam.ac.uk/data_request/cif, or by emailing data_request@ccdc.cam.ac.uk, or by contacting The Cambridge Crystallographic Data Centre, 12 Union Road, Cambridge CB2 1EZ, UK; fax: +44 1223 336033.

AUTHOR INFORMATION

Corresponding Authors

Lin Sun − *Henan Key Laboratory of Polyoxometalate Chemistry, School of Chemistry and Chemical Engineering, Henan University, Kaifeng, Henan 475004, China;* orcid.org/0000-0003-3492-2487; Email: sunlin@vip.henu.edu.cn

Naushad Ahmed − *Department of Chemistry, Indian Institute of Technology Hyderabad, Kandi 502285 Telangana, India;* orcid.org/0000-0002-2671-3581; Email: naushad.chem@gmail.com

Atanu Dey − *Department of Chemistry, Gandhi Institute of Technology and Management (GITAM), Bengaluru 561203 Karnataka, India;* orcid.org/0000-0002-3174-4059; Email: adey2@gitam.edu

Sourav Das − *Department of Basic Sciences, Chemistry Discipline, Institute of Infrastructure Technology Research and Management, Ahmedabad 380026 Gujarat, India;* orcid.org/0000-0002-3346-5598; Email: d.sourav245@gmail.com

Authors

Soumalya Roy − *Department of Basic Sciences, Chemistry Discipline, Institute of Infrastructure Technology Research and Management, Ahmedabad 380026 Gujarat, India*

Jiyuan Du − *Henan Key Laboratory of Polyoxometalate Chemistry, School of Chemistry and Chemical Engineering, Henan University, Kaifeng, Henan 475004, China*

Ezhava Manu Manohar − *Department of Basic Sciences, Chemistry Discipline, Institute of Infrastructure Technology Research and Management, Ahmedabad 380026 Gujarat, India*

Complete contact information is available at: https://pubs.acs.org/10.1021/acs.cgd.2c01226

Notes

The authors declare no competing financial interest.

ACKNOWLEDGMENTS

SD acknowledges the financial support from SERB-DST Early Career Research Award (ECR) with Project Number ECR/2016/001746. Dr. Naushad Ahmed would like to thanks DST-SERB India (File No. PDF/2020/000074) for postdoctoral fellowship. L.S. acknowledge financial support from the National Natural Science Foundation of China (22203027) & Major Project of Science and Technology, Education Department of Henan Province (22A150006).

REFERENCES

(1) Halter, D. P.; Palumbo, C. T.; Ziller, J. W.; Gembicky, M.; Rheingold, A. L.; Evans, W. J.; Meyer, K. Electrocatalytic H2O reduction with f-elements: mechanistic insight and overpotential tuning in a series of lanthanide complexes. *J. Am. Chem. Soc.* **2018**, *140* (7), 2587−2594.

(2) Schmidt, B. M.; Pindwal, A.; Venkatesh, A.; Ellern, A.; Rossini, A. J.; Sadow, A. D. Zwitterionic Trivalent (Alkyl) lanthanide Complexes in Ziegler-Type Butadiene Polymerization. *ACS Catal.* **2019**, *9* (2), 827−838.

(3) Hirai, Y.; Nakanishi, T.; Kitagawa, Y.; Fushimi, K.; Seki, T.; Ito, H.; Hasegawa, Y. Luminescent Europium (III) Coordination Zippers Linked with Thiophene-Based Bridges. *Angew. Chem., Int. Ed.* **2016**, *55* (39), 12059−12062.

(4) Martinić, I.; Eliseeva, S. V.; Nguyen, T. N.; Pecoraro, V. L.; Petoud, S. p. Near-infrared optical imaging of necrotic cells by photostable lanthanide-based metallacrowns. *J. Am. Chem. Soc.* **2017**, *139* (25), 8388−8391.

(5) Moore, E. G.; Samuel, A. P.; Raymond, K. N. From antenna to assay: lessons learned in lanthanide luminescence. *Acc. Chem. Res.* **2009**, *42* (4), 542−552.

(6) Du, Y.; Jiang, Y.; Sun, T.; Zhao, J.; Huang, B.; Peng, D.; Wang, F. Mechanically excited multicolor luminescence in lanthanide ions. *Adv. Mater.* **2019**, *31* (7), 1807062.

(7) Zhu, Z.; Guo, M.; Li, X.-L.; Tang, J. Molecular magnetism of lanthanide: Advances and perspectives. *Coord. Chem. Rev.* **2019**, *378*, 350−364.

(8) Woodruff, D. N.; Winpenny, R. E.; Layfield, R. A. Lanthanide single-molecule magnets. *Chem. Rev.* **2013**, *113* (7), 5110−5148.

(9) Gatteschi, D.; Sessoli, R.; Villain, J.*Molecular nanomagnets*; Oxford University Press on Demand: 2006; Vol. 5.

(10) Sessoli, R.; Gatteschi, D.; Caneschi, A.; Novak, M. Magnetic bistability in a metal-ion cluster. *Nature* **1993**, *365* (6442), 141−143.

(11) Kiefl, E.; Mannini, M.; Bernot, K.; Yi, X.; Amato, A.; Leviant, T.; Magnani, A.; Prokscha, T.; Suter, A.; Sessoli, R. Robust magnetic properties of a sublimable single-molecule magnet. *ACS Nano* **2016**, *10* (6), 5663−5669.

(12) Vincent, R.; Klyatskaya, S.; Ruben, M.; Wernsdorfer, W.; Balestro, F. Electronic read-out of a single nuclear spin using a molecular spin transistor. *Nature* **2012**, *488* (7411), 357−360.

(13) Thiele, S.; Balestro, F.; Ballou, R.; Klyatskaya, S.; Ruben, M.; Wernsdorfer, W. Electrically driven nuclear spin resonance in single-molecule magnets. *Science* **2014**, *344* (6188), 1135−1138.

(14) Leuenberger, M. N.; Loss, D. Quantum computing in molecular magnets. *Nature* **2001**, *410* (6830), 789−793.

(15) Zhang, S.; Cheng, P. Coordination-Cluster-Based Molecular Magnetic Refrigerants. *Chem. Rec.* **2016**, *16* (4), 2077−2126.

(16) Liu, J.-L.; Chen, Y.-C.; Guo, F.-S.; Tong, M.-L. Recent advances in the design of magnetic molecules for use as cryogenic magnetic coolants. *Coord. Chem. Rev.* **2014**, *281*, 26−49.

(17) McAdams, S. G.; Ariciu, A.-M.; Kostopoulos, A. K.; Walsh, J. P.; Tuna, F. Molecular single-ion magnets based on lanthanides and actinides: Design considerations and new advances in the context of quantum technologies. *Coord. Chem. Rev.* **2017**, *346*, 216−239.

(18) Biswas, S.; Goura, J.; Das, S.; Topping, C. V.; Brambleby, J.; Goddard, P. A.; Chandrasekhar, V. Octanuclear heterobimetallic {Ni4Ln4} assemblies possessing Ln4 square grid [2× 2] motifs: synthesis, structure, and magnetism. *Inorg. Chem.* **2016**, *55* (17), 8422−8436.
(19) Schurkus, H. F.; Chen, D.; O'Rourke, M. J.; Cheng, H.-P.; Chan, G. K.-L. Exploring the magnetic properties of the largest single-molecule magnets. *J. Phys. Chem. Lett.* **2020**, *11* (10), 3789−3795.
(20) Wang, W.-M.; Wu, Z.-L.; Cui, J.-Z. Molecular assemblies from linear-shaped Ln 4 clusters to Ln 8 clusters using different β-diketonates: disparate magnetocaloric effects and single-molecule magnet behaviours. *Dalton Trans* **2021**, *50* (37), 12931−12943.
(21) Dey, A.; Das, S.; Kundu, S.; Mondal, A.; Rouzieres, M.; Mathoniere, C.; Clerac, R.; Suriya Narayanan, R.; Chandrasekhar, V. Heterometallic Heptanuclear [Cu5Ln2](Ln= Tb, Dy, and Ho) Single-Molecule Magnets Organized in One-Dimensional Coordination Polymeric Network. *Inorg. Chem.* **2017**, *56* (23), 14612−14623.
(22) Piquer, L. R.; Sañudo, E. C. Heterometallic 3d−4f single-molecule magnets. *Dalton Trans* **2015**, *44* (19), 8771−8780.
(23) Dey, A.; Acharya, J.; Chandrasekhar, V. Heterometallic 3d−4f Complexes as Single-Molecule Magnets. *Chem. Asian J.* **2019**, *14* (24), 4433−4453.
(24) Zabala-Lekuona, A.; Seco, J. M.; Colacio, E. Single-Molecule Magnets: From Mn12-ac to dysprosium metallocenes, a travel in time. *Coord. Chem. Rev.* **2021**, *441*, 213984.
(25) Lin, P. H.; Burchell, T. J.; Ungur, L.; Chibotaru, L. F.; Wernsdorfer, W.; Murugesu, M. A Polynuclear Lanthanide Single-Molecule Magnet with a Record Anisotropic Barrier. *Angew. Chem., Int. Ed.* **2009**, *121* (50), 9653−9656.
(26) Hossain, S.; Das, S.; Chakraborty, A.; Lloret, F.; Cano, J.; Pardo, E.; Chandrasekhar, V. S-shaped decanuclear heterometallic [Ni 8 Ln 2] complexes [Ln (iii)= Gd, Tb, Dy and Ho]: theoretical modeling of the magnetic properties of the gadolinium analogue. *Dalton Trans* **2014**, *43* (26), 10164−10174.
(27) Chandrasekhar, V.; Das, S.; Dey, A.; Hossain, S.; Kundu, S.; Colacio, E. Linear, Edge-Sharing Heterometallic Trinuclear [CoII−LnIII−CoII](LnIII= GdIII, DyIII, TbIII, and HoIII) Complexes: Slow Relaxation of Magnetization in the DyIII Derivative. *Eur. J. Inorg. Chem.* **2014**, *2014* (2), 397−406.
(28) Atanasov, M.; Aravena, D.; Suturina, E.; Bill, E.; Maganas, D.; Neese, F. First principles approach to the electronic structure, magnetic anisotropy and spin relaxation in mononuclear 3d-transition metal single molecule magnets. *Coord. Chem. Rev.* **2015**, *289*, 177−214.
(29) Jiang, S. D.; Wang, B. W.; Su, G.; Wang, Z. M.; Gao, S. A Mononuclear Dysprosium Complex Featuring Single-Molecule-Magnet Behavior. *Angew. Chem., Int. Ed.* **2010**, *122* (41), 7610−7613.
(30) Gómez-Coca, S.; Aravena, D.; Morales, R.; Ruiz, E. Large magnetic anisotropy in mononuclear metal complexes. *Coord. Chem. Rev.* **2015**, *289*, 379−392.
(31) Neese, F.; Pantazis, D. A. What is not required to make a single molecule magnet. *Faraday Discuss.* **2011**, *148*, 229−238.
(32) Sessoli, R.; Powell, A. K. Strategies towards single molecule magnets based on lanthanide ions. *Coord. Chem. Rev.* **2009**, *253* (19−20), 2328−2341.
(33) Ako, A. M.; Hewitt, I. J.; Mereacre, V.; Clérac, R.; Wernsdorfer, W.; Anson, C. E.; Powell, A. K. A ferromagnetically coupled Mn19 aggregate with a record S= 83/2 ground spin state. *Angew. Chem., Int. Ed.* **2006**, *118* (30), 5048−5051.
(34) Bar, A. K.; Kalita, P.; Singh, M. K.; Rajaraman, G.; Chandrasekhar, V. Low-coordinate mononuclear lanthanide complexes as molecular nanomagnets. *Coord. Chem. Rev.* **2018**, *367*, 163−216.
(35) Dey, A.; Kalita, P.; Chandrasekhar, V. Lanthanide (III)-based single-ion magnets. *ACS Omega* **2018**, *3* (8), 9462−9475.
(36) Cremades, E.; Ruiz, E. Mononuclear FeII single-molecule magnets: a theoretical approach. *Inorg. Chem.* **2011**, *50* (9), 4016−4020.
(37) Ungur, L.; Chibotaru, L. F. Strategies toward high-temperature lanthanide-based single-molecule magnets. *Inorg. Chem.* **2016**, *55* (20), 10043−10056.
(38) Biswas, S.; Das, S.; Hossain, S.; Bar, A. K.; Sutter, J. P.; Chandrasekhar, V. Tetranuclear Lanthanide (III) Complexes Containing a Square-Grid Core: Synthesis, Structure, and Magnetism. *Eur. J. Inorg. Chem.* **2016**, *2016* (28), 4683−4692.
(39) Shukla, P.; Pal, T. K.; Sahoo, S. C.; Du, M. H.; Kong, X. J.; Das, S. New Family of Heptanuclear Lanthanide {Ln7} Clusters: Synthesis, Structure, and Magnetic Studies. *ChemistrySelect* **2021**, *6* (9), 2456−2463.
(40) Sorace, L.; Benelli, C.; Gatteschi, D. Lanthanides in molecular magnetism: old tools in a new field. *Chem. Soc. Rev.* **2011**, *40* (6), 3092−3104.
(41) Biswas, S.; Das, S.; Acharya, J.; Kumar, V.; van Leusen, J.; Kögerler, P.; Herrera, J. M.; Colacio, E.; Chandrasekhar, V. Homometallic DyIII complexes of varying nuclearity from 2 to 21: synthesis, structure, and magnetism. *Chem.—Eur. J.* **2017**, *23* (21), 5154−5170.
(42) Das, S.; Dey, A.; Kundu, S.; Biswas, S.; Narayanan, R. S.; Titos-Padilla, S.; Lorusso, G.; Evangelisti, M.; Colacio, E.; Chandrasekhar, V. Decanuclear Ln10 Wheels and Vertex-Shared Spirocyclic Ln5 Cores: Synthesis, Structure, SMM Behavior, and MCE Properties. *Chem.—Eur. J.* **2015**, *21* (47), 16955−16967.
(43) Das, S.; Hossain, S.; Dey, A.; Biswas, S.; Sutter, J.-P.; Chandrasekhar, V. Molecular magnets based on homometallic hexanuclear lanthanide (III) complexes. *Inorg. Chem.* **2014**, *53* (10), 5020−5028.
(44) Biswas, S.; Bejoymohandas, K. S.; Das, S.; Kalita, P.; Reddy, M. L.; Oyarzabal, I.; Colacio, E.; Chandrasekhar, V. Mononuclear lanthanide complexes: energy-barrier enhancement by ligand substitution in field-induced DyIII SIMs. *Inorg. Chem.* **2017**, *56* (14), 7985−7997.
(45) Meng, X.; Wang, M.; Gou, X.; Lan, W.; Jia, K.; Wang, Y.-X.; Zhang, Y.-Q.; Shi, W.; Cheng, P. Two C 2v symmetry dysprosium (iii) single-molecule magnets with effective energy barriers over 600 K. *Inorg. Chem. Front* **2021**, *8* (9), 2349−2355.
(46) Wang, M.; Guo, Y.; Han, Z.; Cheng, X.; Zhang, Y.-Q.; Shi, W.; Cheng, P. Impact of Ligand Substituents on the Magnetization Dynamics of Mononuclear DyIII Single-Molecule Magnets. *Inorg. Chem.* **2022**, *61*, 9785.
(47) Zhang, S.; Wu, H.; Sun, L.; Ke, H.; Chen, S.; Yin, B.; Wei, Q.; Yang, D.; Gao, S. Ligand field fine-tuning on the modulation of the magnetic properties and relaxation dynamics of dysprosium (III) single-ion magnets (SIMs): synthesis, structure, magnetism and ab initio calculations. *J. Mater. Chem. C* **2017**, *5* (6), 1369−1382.
(48) Jiang, Z.; Sun, L.; Yang, Q.; Yin, B.; Ke, H.; Han, J.; Wei, Q.; Xie, G.; Chen, S. Excess axial electrostatic repulsion as a criterion for pentagonal bipyramidal Dy III single-ion magnets with high U eff and TB. *J. Mater. Chem. C* **2018**, *6* (15), 4273−4280.
(49) Roy, S.; Shukla, P.; Prakash Sahu, P.; Sun, Y. C.; Ahmed, N.; Chandra Sahoo, S.; Wang, X. Y.; Kumar Singh, S.; Das, S. Zero-field Slow Magnetic Relaxation Behavior of Dy2 in a Series of Dinuclear {Ln2}(Ln= Dy, Tb, Gd and Er) Complexes: A Combined Experimental and Theoretical Study. *Eur. J. Inorg. Chem.* **2022**, *2022* (5), No. e202100983.
(50) Biswas, S.; Das, S.; Acharya, J.; Kumar, V.; van Leusen, J.; Kögerler, P.; Herrera, J. M.; Colacio, E.; Chandrasekhar, V. Homometallic DyIII complexes of varying nuclearity from 2 to 21: synthesis, structure, and magnetism. *Eur. J. Chem.* **2017**, *23* (21), 5154−5170.
(51) Meng, Y.-S.; Jiang, S.-D.; Wang, B.-W.; Gao, S. Understanding the magnetic anisotropy toward single-ion magnets. *Acc. Chem. Res.* **2016**, *49* (11), 2381−2389.
(52) Le Roy, J. J.; Ungur, L.; Korobkov, I.; Chibotaru, L. F.; Murugesu, M. Coupling strategies to enhance single-molecule magnet properties of erbium−cyclooctatetraenyl complexes. *J. Am. Chem. Soc.* **2014**, *136* (22), 8003−8010.

https://doi.org/10.1021/acs.cgd.2c01226
Cryst. Growth Des. 2023, 23, 1066−1075

(53) Liu, J.; Chen, Y.-C.; Liu, J.-L.; Vieru, V.; Ungur, L.; Jia, J.-H.; Chibotaru, L. F.; Lan, Y.; Wernsdorfer, W.; Gao, S. A stable pentagonal bipyramidal Dy (III) single-ion magnet with a record magnetization reversal barrier over 1000 K. *J. Am. Chem. Soc.* **2016**, *138* (16), 5441−5450.
(54) Zhang, X.; Liu, S.; Vieru, V.; Xu, N.; Gao, C.; Wang, B. W.; Shi, W.; Chibotaru, L. F.; Gao, S.; Cheng, P. Coupling influences SMM properties for pure 4 f systems. *Chem.—Eur. J.* **2018**, *24* (23), 6079−6086.
(55) Ishikawa, N.; Sugita, M.; Ishikawa, T.; Koshihara, S.-y.; Kaizu, Y. Lanthanide double-decker complexes functioning as magnets at the single-molecular level. *J. Am. Chem. Soc.* **2003**, *125* (29), 8694−8695.
(56) Guo, F. S.; Day, B. M.; Chen, Y. C.; Tong, M. L.; Mansikkamäki, A.; Layfield, R. A. A dysprosium metallocene single-molecule magnet functioning at the axial limit. *Angew. Chem., Int. Ed.* **2017**, *129* (38), 11603−11607.
(57) Guo, F.-S.; Day, B. M.; Chen, Y.-C.; Tong, M.-L.; Mansikkamäki, A.; Layfield, R. A. Magnetic hysteresis up to 80 K in a dysprosium metallocene single-molecule magnet. *Science* **2018**, *362* (6421), 1400−1403.
(58) Aravena, D. Ab initio prediction of tunneling relaxation times and effective demagnetization barriers in kramers lanthanide single-molecule magnets. *J. Phys. Chem. Lett.* **2018**, *9* (18), 5327−5333.
(59) Blagg, R. J.; Ungur, L.; Tuna, F.; Speak, J.; Comar, P.; Collison, D.; Wernsdorfer, W.; McInnes, E. J.; Chibotaru, L. F.; Winpenny, R. E. Magnetic relaxation pathways in lanthanide single-molecule magnets. *Nat. Chem.* **2013**, *5* (8), 673−678.
(60) Castro-Alvarez, A.; Gil, Y.; Llanos, L.; Aravena, D. High performance single-molecule magnets, Orbach or Raman relaxation suppression? *Inorg. Chem. Front* **2020**, *7* (13), 2478−2486.
(61) Biswas, S.; Das, S.; Rogez, G.; Chandrasekhar, V. Hydrazone-Ligand-Based Homodinuclear Lanthanide Complexes: Synthesis, Structure, and Magnetism. *Eur. J. Inorg. Chem.* **2016**, *2016* (20), 3322−3329.
(62) Liu, J.-L.; Chen, Y.-C.; Zheng, Y.-Z.; Lin, W.-Q.; Ungur, L.; Wernsdorfer, W.; Chibotaru, L. F.; Tong, M.-L. Switching the anisotropy barrier of a single-ion magnet by symmetry change from quasi-D 5h to quasi-O h. *Chem. Sci.* **2013**, *4* (8), 3310−3316.
(63) Liu, J.-L.; Chen, Y.-C.; Tong, M.-L. Symmetry strategies for high performance lanthanide-based single-molecule magnets. *Chem. Soc. Rev.* **2018**, *47* (7), 2431−2453.
(64) Ungur, L.; Chibotaru, L. F. Magnetic anisotropy in the excited states of low symmetry lanthanide complexes. *Phys. Chem. Chem. Phys.* **2011**, *13* (45), 20086−20090.
(65) Chilton, N. F.; Collison, D.; McInnes, E. J.; Winpenny, R. E.; Soncini, A. An electrostatic model for the determination of magnetic anisotropy in dysprosium complexes. *Nat. Commun.* **2013**, *4* (1), 1−7.
(66) Dong, H.-M.; Liu, Z.-Y.; Tang, H.-M.; Yang, E.-C.; Zhang, Y.-Q.; Zhao, X.-J. Slow relaxation of Dy (iii) single-ion magnets dominated by the simultaneous binding of chelating ligands in low-symmetry ligand-fields. *Dalton Trans* **2022**, *51* (3), 1175−1181.
(67) Ashebr, T. G.; Li, H.; Ying, X.; Li, X.-L.; Zhao, C.; Liu, S.; Tang, J. Emerging Trends on Designing High-Performance Dysprosium (III) Single-Molecule Magnets. *ACS Mater. Lett.* **2022**, *4* (2), 307−319.
(68) Yang, Z.-F.; Tian, Y.-M.; Zhang, W.-Y.; Chen, P.; Li, H.-F.; Zhang, Y.-Q.; Sun, W.-B. High local coordination symmetry around the spin center and the alignment between magnetic and symmetric axes together play a crucial role in single-molecule magnet performance. *Dalton Trans* **2019**, *48* (15), 4931−4940.
(69) Sun, W.-B.; Yan, P.-F.; Jiang, S.-D.; Wang, B.-W.; Zhang, Y.-Q.; Li, H.-F.; Chen, P.; Wang, Z.-M.; Gao, S. High symmetry or low symmetry, that is the question−high performance Dy (III) single-ion magnets by electrostatic potential design. *Chem. Sci.* **2016**, *7* (1), 684−691.
(70) Chen, Y.-C.; Liu, J.-L.; Ungur, L.; Liu, J.; Li, Q.-W.; Wang, L.-F.; Ni, Z.-P.; Chibotaru, L. F.; Chen, X.-M.; Tong, M.-L. Symmetry-supported magnetic blocking at 20 K in pentagonal bipyramidal Dy (III) single-ion magnets. *J. Am. Chem. Soc.* **2016**, *138* (8), 2829−2837.
(71) Brzozowska, M.; Handzlik, G.; Kurpiewska, K.; Zychowicz, M.; Pinkowicz, D. Pseudo-tetrahedral vs. pseudo-octahedral Er III single molecule magnets and the disruptive role of coordinated TEMPO radical. *inorg. Chem. Front* **2021**, *8* (11), 2817−2828.
(72) Orlova, A. P.; Hilgar, J. D.; Bernbeck, M. G.; Gembicky, M.; Rinehart, J. D. Intuitive Control of Low-Energy Magnetic Excitations via Directed Dipolar Interactions in a Series of Er (III)-Based Complexes. *J. Am. Chem. Soc.* **2022**, *144*, 11316.
(73) Cai, X.; Cheng, Z.; Wu, Y.; Jing, R.; Tian, S.-Q.; Chen, L.; Li, Z.-Y.; Zhang, Y.-Q.; Cui, H.-H.; Yuan, A. Tuning the Equatorial Negative Charge in Hexagonal Bipyramidal Dysprosium (III) Single-Ion Magnets to Improve the Magnetic Behavior. *Inorg. Chem.* **2022**, *61* (8), 3664−3673.
(74) Mondal, A.; Konar, S. Effect of an axial coordination environment on quantum tunnelling of magnetization for dysprosium single-ion magnets with theoretical insight. *Dalton Trans* **2022**, *51* (4), 1464−1473.
(75) Rinehart, J. D.; Long, J. R. Exploiting single-ion anisotropy in the design of f-element single-molecule magnets. *Chem. Sci.* **2011**, *2* (11), 2078−2085.
(76) Zhang, P.; Zhang, L.; Wang, C.; Xue, S.; Lin, S.-Y.; Tang, J. Equatorially coordinated lanthanide single ion magnets. *J. Am. Chem. Soc.* **2014**, *136* (12), 4484−4487.
(77) Zhang, H.; Nakanishi, R.; Katoh, K.; Breedlove, B. K.; Kitagawa, Y.; Yamashita, M. Low coordinated mononuclear erbium (iii) single-molecule magnets with C 3v symmetry: a method for altering single-molecule magnet properties by incorporating hard and soft donors. *Dalton Trans* **2018**, *47* (2), 302−305.
(78) Li, J.; Kong, M.; Yin, L.; Zhang, J.; Yu, F.; Ouyang, Z.-W.; Wang, Z.; Zhang, Y.-Q.; Song, Y. Photochemically Tuned Magnetic Properties in an Erbium (III)-Based Easy-Plane Single-Molecule Magnet. *Inorg. Chem.* **2019**, *58* (21), 14440−14448.
(79) Dong, Y.; Zhu, L.; Yin, B.; Zhu, X.; Li, D. Regulating the magnetic properties of seven-coordinated Dy (III) single-ion magnets through the effect of positional isomers on axial crystal-field. *Dalton Trans* **2021**, *50* (46), 17328−17337.
(80) *SSRM version 6.45*; Bruker Analytical X-ray Systems, Inc.; Madison, WI, 2003.
(81) Sheldrick, G.*SADABS, software for empirical absorption correction, Ver. 2.05*; University of Göttingen; Göttingen, Germany, 2002.
(82) *SHELXTL Reference Manual, Ver. 6.1*; Bruker Analytical X-ray Systems, Inc., Madison, WI, 2000; Vol. *71* (1), pp 3−8.
(83) Sheldrick, G. M. A short history of SHELX. *Acta Crystallographica Section A: Foundations of Crystallography* **2008**, *64* (1), 112−122.
(84) Dolomanov, O. V.; Bourhis, L. J.; Gildea, R. J.; Howard, J. A.; Puschmann, H. OLEX2: a complete structure solution, refinement and analysis program. *Journal of applied crystallography* **2009**, *42* (2), 339−341.
(85) Bradenburg, K.; Putz, H. J. C. I. G. B. Germany, Diamond, version 3.1 e. 2005.
(86) Ramírez-Jiménez, A.; Gómez, E.; Hernández, S. Penta-and heptacoordinated tin (IV) compounds derived from pyridine Schiff bases and 2-pyridine carboxylate: Synthesis and structural characterization. *J. Organomet. Chem.* **2009**, *694* (18), 2965−2975.
(87) Ramírez-Jiménez, A.; Gómez, E.; Hernández, S. Penta-and heptacoordinated tin (IV) compounds derived from pyridine Schiff bases and 2-pyridine carboxylate: Synthesis and structural characterization. *J. Organomet. Chem.* **2009**, *694* (18), 2965−2975.
(88) Jin, P. B.; Yu, K. X.; Luo, Q. C.; Liu, Y. Y.; Zhai, Y. Q.; Zheng, Y. Z. Tetraanionic arachno-Carboranyl Ligand Imparts Strong Axiality to Terbium (III) Single-Molecule Magnets. *Angew. Chem., Int. Ed.* **2022**, *61*, No. e202203285.
(89) Li, Z. H.; Zhai, Y. Q.; Chen, W. P.; Ding, Y. S.; Zheng, Y. Z. Air-Stable Hexagonal Bipyramidal Dysprosium (III) Single-Ion

Magnets with Nearly Perfect D6h Local Symmetry. *Chem.—Eur. J.* **2019**, *25* (71), 16219−16224.
(90) Canaj, A. B.; Dey, S.; Martí, E. R.; Wilson, C.; Rajaraman, G.; Murrie, M. Insight into D6h Symmetry: Targeting Strong Axiality in Stable Dysprosium (III) Hexagonal Bipyramidal Single-Ion Magnets. *Angew. Chem., Int. Ed.* **2019**, *58* (40), 14146−14151.
(91) Norre, M. S.; Gao, C.; Dey, S.; Gupta, S. K.; Borah, A.; Murugavel, R.; Rajaraman, G.; Overgaard, J. High-Pressure Crystallographic and Magnetic Studies of Pseudo-D 5 h Symmetric Dy (III) and Ho (III) Single-Molecule Magnets. *Inorg. Chem.* **2020**, *59* (1), 717−729.
(92) Ding, X. L.; Zhai, Y. Q.; Han, T.; Chen, W. P.; Ding, Y. S.; Zheng, Y. Z. A local D4h symmetric dysprosium (III) single-molecule magnet with an energy barrier exceeding 2000 K. *Chem.—Eur. J.* **2021**, *27* (8), 2623−2627.
(93) Bala, S.; Huang, G.-Z.; Ruan, Z.-Y.; Wu, S.-G.; Liu, Y.; Wang, L.-F.; Liu, J.-L.; Tong, M.-L. A square antiprism dysprosium single-ion magnet with an energy barrier over 900 K. *ChemComm* **2019**, *55* (67), 9939−9942.
(94) Casanova, D.; Llunell, M.; Alemany, P.; Alvarez, S. The rich stereochemistry of eight-vertex polyhedra: a continuous shape measures study. *Chem.—Eur. J.* **2005**, *11* (5), 1479−1494.
(95) Singh, S. K.; Prabusankar, G. Ln (III)(Ln= La, Gd, and Dy) Benzimidazolium Tricarboxylate Coordination Polymers with Hydrogen Bonding Modulated Magnetic Relaxation. *Cryst. Growth Des* **2022**, *10* (16), 6046−6055.
(96) Yeşilbağ, S.; Çınar, E. B.; Dege, N.; Ağar, E.; Saif, E. Crystal structure and Hirshfeld surface analysis of dimethyl 3, 3′-{[(1E, 2E)-ethane-1, 2-diylidene] bis (azanylylidene)} bis (4-methylbenzoate). *Acta Crystallogr. E: Crystallogr. Commun.* **2022**, *78* (4), 340.
(97) Du, J.; Duan, B.; Gao, L.; Jiang, Z.; Sun, L.; Ma, P.; Li, M. A centrosymmetric Dy2 compound derived from acylhydrazone Schiff base ligand exhibiting zero-field single-molecule magnet behavior. *J. Mol. Struct.* **2022**, *1252*, 132223.
(98) Chen, H.; Sun, L.; Zhang, J.; Xiao, Z.; Ma, P.; Wang, J.; Zhang, Y.; Niu, J. Magnetic field and dilution effects on the slow relaxation of {Er 3} triangle-based arsenotungstate single-molecule magnets. *Dalton Trans* **2020**, *49* (35), 12458−12465.
(99) Zhang, S.; Mo, W.; Zhang, J.; Zhang, Z.; Yin, B.; Hu, D.; Chen, S. Regulation of substituent effects on configurations and magnetic performances of mononuclear DyIII single-molecule magnets. *Inorg. Chem.* **2019**, *58* (22), 15330−15343.
(100) Zheng, Y. Z.; Lan, Y.; Wernsdorfer, W.; Anson, C. E.; Powell, A. K. Polymerisation of the Dysprosium Acetate Dimer Switches on Single-Chain Magnetism. *Chem.—Eur. J.* **2009**, *15* (46), 12566−12570.
(101) Sun, L.; Zhang, S.; Qiao, C.; Chen, S.; Yin, B.; Wang, W.; Wei, Q.; Xie, G.; Gao, S. Fine-Tuning of the Coordination Environment To Regulate the Magnetic Behavior in Solvent/Anion-Dependent DyIII Compounds: Synthesis, Structure, Magnetism, and Ab Initio Calculations. *Inorg. Chem.* **2016**, *55* (20), 10587−10596.
(102) Jiang, Z.; Sun, L.; Li, M.; Wu, H.; Xia, Z.; Ke, H.; Zhang, Y.; Xie, G.; Chen, S. Solvent-tuned magnetic exchange interactions in Dy 2 systems ligated by a μ-phenolato heptadentate Schiff base. *RSC Adv.* **2019**, *9* (68), 39640−39648.
(103) Zhang, S.; Ke, H.; Liu, X.; Wei, Q.; Xie, G.; Chen, S. A nine-coordinated dysprosium (III) compound with an oxalate-bridged dysprosium (III) layer exhibiting two slow magnetic relaxation processes. *ChemComm* **2015**, *51* (82), 15188−15191.
(104) Liu, J.-L.; Yuan, K.; Leng, J.-D.; Ungur, L.; Wernsdorfer, W.; Guo, F.-S.; Chibotaru, L. F.; Tong, M.-L. A six-coordinate ytterbium complex exhibiting easy-plane anisotropy and field-induced single-ion magnet behavior. *Inorg. Chem.* **2012**, *51* (15), 8538−8544.
(105) Yin, C.-L.; Hu, Z.-B.; Long, Q.-Q.; Wang, H.-S.; Li, J.; Song, Y.; Zhang, Z.-C.; Zhang, Y.-Q.; Pan, Z.-Q. Single molecule magnet behaviors of Zn 4 Ln 2 (Ln= Dy III, Tb III) complexes with multidentate organic ligands formed by absorption of CO 2 in air through in situ reactions. *Dalton Trans* **2019**, *48* (2), 512−522.
(106) Cole, K. S.; Cole, R. H. Dispersion and absorption in dielectrics I. Alternating current characteristics. *J. Chem. Phys.* **1941**, *9* (4), 341−351.
(107) Acharya, J.; Ahmed, N.; Gonzalez, J. F.; Kumar, P.; Cador, O.; Singh, S. K.; Pointillart, F.; Chandrasekhar, V. Slow magnetic relaxation in a homo dinuclear Dy (III) complex in a pentagonal bipyramidal geometry. *Dalton Trans* **2020**, *49* (37), 13110−13122.
(108) Yi, X.; Bernot, K.; Cador, O.; Luzon, J.; Calvez, G.; Daiguebonne, C.; Guillou, O. Influence of ferromagnetic connection of Ising-type Dy III-based single ion magnets on their magnetic slow relaxation. *Dalton Trans* **2013**, *42* (19), 6728−6731.
(109) Katoh, K.; Kajiwara, T.; Nakano, M.; Nakazawa, Y.; Wernsdorfer, W.; Ishikawa, N.; Breedlove, B. K.; Yamashita, M. Magnetic Relaxation of Single-Molecule Magnets in an External Magnetic Field: An Ising Dimer of a Terbium (III)−Phthalocyaninate Triple-Decker Complex. *Chem.—Eur. J.* **2011**, *17* (1), 117−122.
(110) Aquilante, F.; Autschbach, J.; Carlson, R. K.; Chibotaru, L. F.; Delcey, M. G.; De Vico, L.; Galván, I.; Ferré, N.; Frutos, L. M.; Gagliardi, L.*Molcas 8: New capabilities for multiconfigurational quantum chemical calculations across the periodic table*; Wiley Online Library: 2016; Vol. *37*.

https://doi.org/10.1021/acs.cgd.2c01226
Cryst. Growth Des. 2023, 23, 1066−1075